TUTDoR

Optimization of spark plasma sintering parameters of inconel 738LC alloy using response surface methodology (RSM).

Item Type	Article
Authors	Ogunbiyi, Olugbenga;Jamiru, Tamba
DOI	https://doi.org/10.1016/j.ijlmm.2019.10.002
Publisher	Elsevier
Rights	Attribution-NonCommercial-ShareAlike 4.0 International
Download date	2025-12-06 15:52:26
Item License	http://creativecommons.org/licenses/by-nc-sa/4.0/
Link to Item	https://hdl.handle.net/20.500.14519/2275

International Journal of Lightweight Materials and Manufacture 3 (2020) 177–188

Contents lists available at ScienceDirect

International Journal of Lightweight Materials and Manufacture

journal homepage: https://www.sciencedirect.com/journal/international-journal-of-lightweight-materials-and-manufacture

Original Article

Optimization of spark plasma sintering parameters of inconel 738LC alloy using response surface methodology (RSM)

Olugbenga Ogunbiyi [a, *], Tamba Jamiru [a], Rotimi Sadiku [b], Oluwagbenga Adesina [a], Jimmy lolu Olajide [a], Lodewyk Beneke [a]

[a] Department of Mechanical Engineering, Mechatronics and Industrial Design, Tshwane University of Technology, Pretoria, South Africa
[b] Institute for NanoEngineering Research (INER), Department of Chemical, Metallurgical and Materials Engineering, Tshwane University of Technology, Pretoria, South Africa

ARTICLE INFO

Article history:
Received 30 August 2019
Received in revised form
7 October 2019
Accepted 8 October 2019
Available online 19 October 2019

Keywords:
Optimization
IN738LC alloy
Density
Hardness
Temperature
Pressure

ABSTRACT

The quality and properties of a material can be improved by the choice of processing technique adopted. This study investigates the influence of process parameters of spark plasma sintering (SPS) method on the densification and microhardness properties of IN738LC superalloy. In order to reduce the numbers of experiments and eliminate trial by error approach, design of experiment (DOE) approach was adopted. This involved the use of response surface methodology and central composite design (CCD) with temperature and pressure as the SPS experimental variables. Analysis of the variance (ANOVA) was studied to validate the developed model, coupled with understanding the influence of individual variable and their combined interaction on the output (responses). In this case, the responses were the density and the hardness properties. The data obtained from the numerically predicted values and the physical experiment was statistically examined to obtain a predictive model which harmonizes the density and the hardness as a function of the independent operation parameters. Empirical models were developed for the responses and fifteen solution runs was processed to establish whose response desirability is closest to 1. It was observed that SPS processing temperature (variable) have a major effect on the responses and the most desired temperature is 1200 °C at 50 MPa pressure. Under this condition, the hardness is 362.028 HV and the corresponding percentage relative density id 98.457% (7.772 g/cm^3). The theoretical density is given as 7.894 g/cm^3.
© 2019 The Authors. Production and hosting by Elsevier B.V. on behalf of KeAi Communications Co., Ltd. This is an open access article under the CC BY-NC-ND license (http://creativecommons.org/licenses/by-nc-nd/4.0/).

1. Introduction

Superalloys are high-strength and high performing material, together with possessing characteristics such as excellent mechanical properties, resistance to corrosion, good creep and fatigue strength (even at elevated temperature). Over the years, steels have been the most used material in the industries for structural applications, especially in the aerospace, chemical, oil and gas, marine, automobile, power plants and metal fabrication industries [1,2]. Owing to various applications of steels, especially for high temperature applications, challenges have risen, and these have placed demand on engineers to find alternative high-performing materials. Among several limitations of steels, sudden softening at elevated temperature is a major problem and has reduced its applications in a high temperature environment [3]. The challenges resulted to the development of superalloys. Several industries use superalloys for different components, however, aerospace and land-based power plant (turbine system) industries dominated in superalloys consumption. Therefore, it is imperative to use materials of good qualities that can withstand the aggressive operation conditions of high temperature environment in order to improve the efficiency and performance of the turbine system. Materials used in such extreme conditions (hot gas/steam path) must possess high mechanical strength including good creep, fatigue, corrosion and oxidation resistance properties. Based on these conditions, nickel based superalloys to be precise, are material of choice [4]. They are critical alloys that possess good strength at high operating temperatures close to their melting temperature. They are known

* Corresponding author.
E-mail address: olugbengaogunbiyi@gmail.com (O. Ogunbiyi).
Peer review under responsibility of Editorial Board of International Journal of Lightweight Materials and Manufacture.

https://doi.org/10.1016/j.ijlmm.2019.10.002
2588-8404/© 2019 The Authors. Production and hosting by Elsevier B.V. on behalf of KeAi Communications Co., Ltd. This is an open access article under the CC BY-NC-ND license (http://creativecommons.org/licenses/by-nc-nd/4.0/).

to possess consistent functional properties over a wide range of operational temperatures, usually between −217 °C to 1300 °C. Thus, they function in cryogenic environment, elevated temperature environment and area where they are susceptible to chemical attack such as nuclear reactor and petrochemical environment. The breakthrough in the development of superalloy has compensated for the shortcomings often faced by using steels.

There are several types of nickel-based superalloys (Inconel, Rene alloys, Hastelloy, TMS alloys, Waspaloy, MP98T and CMSX single crystal alloys) [5] and the phases present largely depend on the alloy composition. Inconel 738 low carbon (IN738LC) belongs to the group of nickel-based superalloy that is used for various applications in engineering, especially in an aggressive environment such as turbine operations [6–8]. They possessed high strength and this is attributed to the Face Centered Cubic (FCC) crystal structure of the gamma (γ) matrix phase and the ordered intermetallic gamma prime (γ'-addition of aluminium and titanium) phase. However, the formation of other phases such as gamma prime (γ"-addition of niobium and vanadium), carbide and precipitate solid solution (chromium, molybdenum, tantalum, cobalt e.t.c) greatly depend on the alloy composition and demand for specific properties in relation to area of application. Therefore, understanding the effects of the alloying elements to the development of specific microstructure characteristic is imperative [9]. The high strength γ phase (FCC lattice structure) surrounds the γ' or γ" precipitate cubic lattice phase in its microstructure formation. Chen et al. [4] reported that, a nickel based superalloy should only be considered for fabricating a turbine blade if the γ' phase fraction is more than 0.6 of the total fraction of phases present. Due to the intricacies involved in the fabrication processes of superalloys and desire to obtain material with good structural integrity, powder metallurgy (PM) method has become a better choice, compared to conventional liquid melting and investment casting methods. There are different methods that are available in PM which include injection moulding, selective laser melting, hot press, microwave sintering, hot isostatic pressing and more recent spark plasma sintering (SPS). However, the latter have several advantages over those other mentioned methods.

SPS advantages include, fast sintering process (between 5 and 40 min), minimal grain growth, sintering without the use of binders, easy operation with minimal human interference, combined consolidation and sintering in one single operation. Furthermore, its present opportunity for manufacturing different class of materials (metals, metal alloys, composites, ceramics and to more recent polymers) and is energy efficient [10]. However, this is not to say that SPS is a perfect powder sintering method, the issue of handling irregular shape still remains unresolved and the pulsed DC generator is expensive. Also, there is a wider conflict in the research findings on the mechanism of SPS [11,12]. Attempt has been made to fabricate complex shapes with SPS [13,14] and even though success was recorded, this still require further investigation. Among several descriptions of SPS, Suarez et al. [15], succinctly describe SPS as a fast sintering technique where heat is rapidly and homogenously distributed to the powder body. The heat supplied through the pulsed direct electric current of low voltage and the applied force through a uniaxial piston under low atmospheric pressure are used to consolidate powder materials. The joule heat generated is delivered to the powder compact at a macroscopic level, that is, directly to the particles and particles contact points where the energy is required. The application of high sintering temperature, pressure and heating rate promotes fast sintering processes and manufacturing of highly densified materials. Hence, such material possesses excellent mechanical, thermal and chemical properties coupled with minimal microstructural defects. SPS also minimizes impurities inclusion such as oxygen and hydrogen.

In simplifying the manufacturing processes of materials, optimization of processing parameters is imperative for better material properties and to minimizing unnecessary trial by error approach. Thus, design of experiment (DOE) model has come in handy and provided solution to these challenges. DOE is a statistical model approach that encompasses production planning, managing, analyzing and interpreting controlled operations, in order to establish the optimum range of process that controls specific material properties. It is useful for different experimental situations and present at a glance, the effect of possible parameter's combination on the obtained output (response). Therefore, DOE approach helps to standardize production processes, reduces operational cost, minimizes wastage, saves energy, saves time and ensure accurate results in experimental studies. The accurate selection of process parameters resulted to fabrication of alloy with refined microstructure. Defect such as pores, pin holes and segregation are greatly reduced. Surprisingly, literature have not widely documented the use of SPS for the fabricating IN738 LC superalloy which justify the need for DOE approach for SPS fabrication of IN738LC alloy. Furthermore, it is imperative to state that; process optimization helps in the selection of processing parameters that gives densification close to theoretical density and by extension translating to manufacturing material with good properties.

Ujah et al. [16], in their study on the optimization of SPS parameters of Al-CNTs-Nb nano-composite, using Taguchi design of experiment. The sintering temperature, pressure, heating rate and holding time was optimized. There was close agreement between DOE results (Taguchi predicted result) and experimental results (density and hardness). Taguchi method is another DOE statistical model that is used for processes optimization. Mohammadzadeh et al. [17], worked on optimization of physical and mechanical properties of SPSed titanium and titanium diboride composite. They used Response Surface Methodology (RSM) DOE for the study. The experiments were conducted based on the factorial design obtained from the RSM report. It was reported that sintering temperature among the parameters used has dominant effect on the obtained density, porosity and hardness properties. Literature are available on the optimization of process parameters of SPS using RSM approach, although not on IN738LC superalloy fabrication by SPS [18–23]. This study attempts to fabricate Inconel 738LC superalloy by optimizing the SPS processing parameters using RSM design of experiment (DOE) and analysis of variance (ANOVA) statistical tool. This in turn, will reduce numbers of experimental runs and material wastage.

2. Materials and methods

2.1. Materials and samples preparation

Alloys were formed by blending seven elemental powders together. The starting powder comprises of nickel (TLS-Technik Gmbh, 99.5% purity), chromium and cobalt (Alfa Aesar, 99.9% purity), titanium, tungsten and tantalum (Sigma Aldrich, 99.5% purity) and aluminium (TLS-Technik Gmbh, 99.5% purity). The powders were weighed by using an electronic digital weighing balance with a tolerance of ± 0.001 g. The IN738LC alloy composition in weight percent is shown in Table 1.

Table 1
Percentage weight of IN738LC alloy composition.

Elements	Ni	Cr	Co	Ti	Al	Ta	W
wt%	64.58	16	8.3	3.4	3.4	1.72	2.6
Particle size (μm)	45–90	≤ 44	≤ 44	≤ 44	25	≤ 44	≤ 44

The samples composition ratio is based on the investigation conducted on a failed turbine blade [8]. The green powders were prepared by pre-alloying process, using a tubular shaker mixer model T2F at a mixing speed of 49 rpm for a period of 12 h in a dry environment. Tungsten balls (8 mm diameter) were incorporated into the powder's plastic container during the alloying process and in the ratio of 10:1 (ball-to-powder) in order to ensure homogenous distribution of powder particles.

2.2. Fabrication of IN738LC alloys

Pre-alloyed powders were transferred into a prepared graphite mould and afterwards placed in the heating chamber of SPS furnace. A 59.3 g of admixed powder was poured into the graphite mould. This was the calculated amount of powder required to produce Ø40 by 6 mm thickness sintered alloys. Prior to this, a LAB mini press machine was used to manually compact (cold compaction) the green powders in the mould, in order to ensure that air is removed from the body of the compact. The graphite mould has an internal diameter of 40 ± 0.05 mm, external diameter of 60 ± 0.01 mm and a height of 48 mm. The internal surface of the dies and the surface of the punches (both upper and lower) that made contact with the green powder were lined with graphite papers of 0.3 mm thickness. This is to prevent reaction between the mould (die and punches) and the sample during sintering, especially at high temperatures and also to ensure easy removal of sintered sample. The green powders were sintered using HPD 25 spark plasma sintering (SPS) machine (FCT system, Raustein, Germany). The SPS machine was set to operate at vacuum pressure of 0.605 mbar (46.09%), absolute pressure of 1.2 mbar (120 Pa) and relative pressure of −convert 500 mbar (50,000 Pa). The alloys fabricated and the designed parameters used are presented in Table 2. The sintering temperature and pressure were varied while the heating rate was fixed at 100 °C/min and soaking time fixed at 5 min. At the end of the sintering process, when the desired set temperature and soaking time have been achieved, the current was switched off and the sample was cooled to room temperature (22 °C). The sintering operations was repeated to get the required number of samples. The samples were sand blasted to remove any form of graphite deposition on their surface and further preparation ensue (metallographic examination). The SPS machine, die, punches, sintered samples and schematic diagram of SPS system are presented in Figs. 1–3.

Table 2
Experimental design and actual response results of density and microhardness of IN738LC alloy.

Runs	Factors		Response 1		Response 2
	Temperature A (°C)	Pressure B (MPa)	Density (%)	Density (g/cm^3)	Hardness (HV)
1	1000	30	91.4	7.215	306.9
2	1000	40	92.1	7.270	306.98
3	1000	50	92.8	7.325	307.68
9	1100	30	95.2	7.515	333.89
4	1100	40	96	7.578	334.2
6	1100	40	96	7.578	334.2
7	1100	40	96	7.578	334.2
8	1100	40	96	7.578	334.2
10	1100	40	96	7.578	334.2
5	1100	50	96.5	7.617	334.5
11	1200	30	98.2	7.752	360.15
12	1200	40	98.3	7.760	362.2
13	1200	50	98.4	7.768	362.25

Fig. 1. Image of the SPS machine used.

2.3. Density measurement

The bulk density of the starting powders was calculated according to Equation (1) and the experimental densities were measured by using Archimedes principle. Rule of mixtures was used to calculate the relative densities of the sintered samples with reference to the starting powders theoretical bulk density.

$$\rho bulk = \left(\frac{\%Ni}{\rho Ni} + \frac{\%Cr}{\rho Cr} + \cdots\cdots + \frac{\%n!}{\rho n!}\right)^{-1} \quad (1)$$

where $\rho bulk$ is the total bulk density of the starting powder (g/cm^3), ρNi, ρCr and $\rho n!$ are bulk densities of individual element (powder) and $\%Ni$, $\%Cr$ and $\%n!$ are the percentage composition of the elements present in the alloy. The theoretical density was calculated to be 7.894 g/cm^3.

2.4. Microhardness testing

The Vicker's micro-hardness (HV) tester (Future-tech, 800) was used to test the micro-hardness property of the sintered alloys using a diamond indenter. The test parameters include: a load of 100 g force (1.0 N), dwell time of 15 s and spacing of 0.1. The experiment was conducted at room temperature (22 °C) and it was repeated ten times for each sample. The indented points were representation of the microstructure features observed from the alloys which include, the grain, grain boundary and the solid solution precipitates. The test results were recorded, and the arithmetic mean of the ten successful indentation was taken as the actual micro-hardness value.

2.5. Microstructural characterization

Samples sectioning was conducted to obtain a test specimen for microstructure analysis. The sectioned samples were grinded using silicon carbide papers (320, 600, 800 and 1200 grit sizes) and polished by using diamond paste (diamaxx: mono 9 μm). In order to obtain a mirror like surface finish, alumina powder was applied during the final stage of polishing. The unetched surface was examined under SEM machine, incorporated with an EDS detector and INCA X-Stream2 pulse analyzer software in order to obtain the microstructure features.

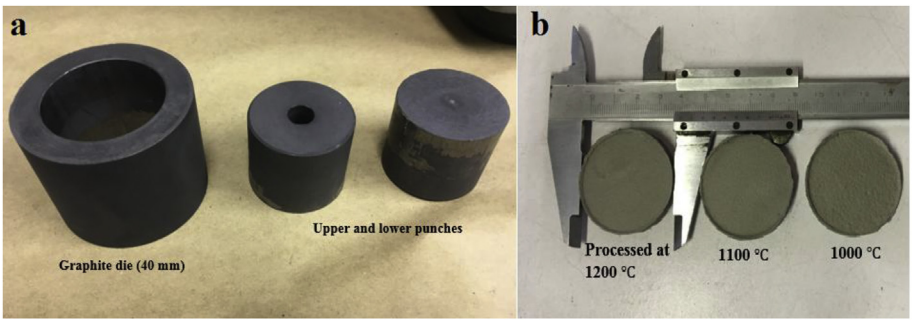

Fig. 2. (a) Image of the die and punches used (b) images of the samples for the optimized sintering temperature.

2.6. Design of numerical experiment

Design of experiment (DOE) is a statistical model introduced by R.A. Fisher in 1920s [24], to determine the effects individual parameter and interactions between parameters on the output of any design. DOE technique is suitable for manufacturing processes and helps to reduce production cost, saves time, reduce test duplication (numbers of iterations) and waste. Hence, it is a good tool for the optimization of process design, minimization of labour complexity, improving product quality (performance consistency) and variation reduction [25]. DOE is used in this study to evaluate the influence of spark plasma sintering parameters on the microhardness and densification behaviour of IN738LC superalloy. The design expert (version 8, stat-ease software) was used to generate the statistical data and the regression model for the experiment. These were studied by using response surface methodology and central composite design (CCD) for process optimization. Factors such as processing temperatures (A) and pressures (B) were considered while the hardness and densification were the experimental responses. The total number of runs obtained using DOE approach was thirteen (RSM and CCD method).

2.7. The response surface methodology

RSM is a statistical and mathematical model used for analyzing experimental problems by optimizing the process parameters in which the influence of different variables are evaluated on a response of interest [26]. Therefore, RSM afford opportunity to determine the functional relationships between the processing parameters (temperature and pressure) and the material properties responses (density and hardness) of sintered IN738LC alloys. RSM method among several other experimental design techniques is known for its ability to present clear understanding of interactions between variables. More importantly, is the ability to give precise and accurate data with reduced number of experimental runs [27]. In addition, the CCD which is commonly used to build the second-order model is very versatile, suitable, highly structured and diversified design model for locating the optimum point(s) and the interaction effects between variables. The sintering temperature and pressure were varied for the predictor variables. The microhardness and density formed the response variables in the RSM model. For this study, factors are varied over three levels: the high level (+1), low level (−1) and center points (0). This is presented in Table 3.

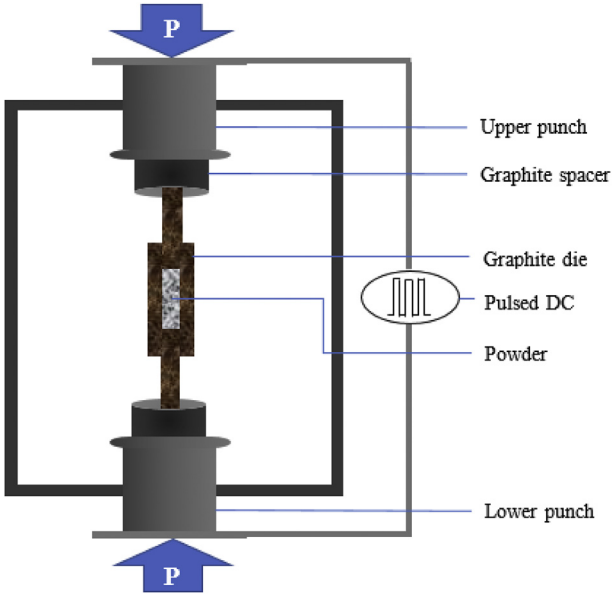

Fig. 3. Schematic diagram of SPS system.

The selection of suitable values for the two variables, that is, range of sintering temperature and pressure were obtained from literature [28]. The sintering temperature range (850–1200 °C) was found beneficial for spark plasma sintered superalloys [29]. Therefore, sintering temperature range between 1000 and 1200 °C was set for this experiment. This is because, it was reported that higher sintering temperature gives better densification and hardness properties [30]. This study aimed at investigating the effect of individual variable and simultaneous combinations of variables (temperature and pressure) on the SPSed 1N738LC alloys response (maximum responses: density and hardness). The experimental runs (number) generated using RSM is calculated using Equation (2).

$$N = 2^n + 2n + n_c \tag{2}$$

where N is the total number of experimental runs, n is the number of variables and n_c is the number of replicates at center point.

2.8. Analysis of variance

The variance (ANOVA) analysis is conducted on the modified models as suggested by the statistical tool. The F test (for F and P

Table 3
Independent variables: symbols, levels and values in the experimental design of IN738LC alloy.

Symbols	Variables	Levels		
		−1	0	1
A	Sintering temperature (°C)	1000	1100	1200
B	Pressure (MPa)	30	40	50

values) is conducted by using the statistical tool to determine the influence of factors and interactive influence of variables. The ANOVA helps to identify differences in data obtained and separate into components. This mean that values characteristics are calculated individually and presented in the ANOVA table for all terms that appear in the model equations [31]. Several parameters are used to ascertain the authenticity of the suggested models, especially the accuracy of the obtained values as compare to experimental data. These includes coefficient of determination (R^2), coefficient of variation (C.V.), adequate precision, adjusted coefficient of determination (Adj. R^2) and lack of fit (LOF). The two values that signifies that a model can be considered significant are the R^2 and Adj. R^2. Also, a model with a small p-value (<0.05) and a large *F*-value (>unity) is considered significant [32]. The present study show that the R^2 values were closer to 1, this signifies that the calculated results and the experimental results are in good agreement within the range of the experiment. The residual variability in the data as a percentage of the mean of the response variable is measured by the coefficient of variant (C.V.). The "Pure Error" and the residual error is compared using the Lack of Fit (LOF) values, from the repeated experimental design points. The 3D mapping is used to predict the influence of individual variable independently and their interactions on the obtained responses. The analysis of variance (ANOVA) is presented in section 3.

3. Results and discussion

3.1. Experimental results and analysis

The full detail of the experimental design comprising of three-level-two factor central composite design model including their responses (hardness and density) from the physical experiment is represented in Table 2. It was ensured that the selected values of variables were within the specified range of the experimental design. A total test of 13 runs were performed for optimizing the two variables and their corresponding effects on the obtained responses (density and hardness) was investigated. The choice of the sintering temperature range for this experiment is based on similar work reported in literature and it was reported that lower sintering temperature resulted to less dense materials [33]. Sintering temperature below 950 °*C* may not be suitable for this type of alloy, moreso, with the presence of tungsten (3422 °C) and tantalum (3017 °C) which has high melting temperatures [34]. The other elements present in the alloy have a melting temperature that is less than 2000 °C. Therefore, high sintering temperature is required to enable reaction (diffusion) of these two alloying elements [35]. Moreover, high sintering temperature have been reported to contribute immensely to high densification and high hardness properties of sintered superalloys with marginal recorded percentage porosity [10].

3.2. Response surface methodology of IN738LC properties

The RSM with CCD was used to evaluate levels of factors and the degree of their interactions on the properties of IN738LC superalloy. Furthermore, a mathematical model was obtained from the ANOVA analysis using a statistical model approach. The model harmonized the relationship between the two independent process variables (temperature and pressure) and the predicted response (density and hardness). The regression provides better understanding of the relationship between IN738LC alloy and its sintering parameters (pressure and temperature). The test conducted explained the significance of individual model coefficient, regression model and lack of fit. These parameters are used to determine the effectiveness of the model and its predictive ability. The ANOVA model for the density which is the test results, including the statistical parameters of the model equation is presented in Tables 4 and 5 respectively.

3.3. ANOVA analysis and model fitting for IN738LC alloy density measurement

The *F* value from the results presented in Table 4 is 868.04 and this implies that the model is significant. Noise could not be attributed to the high value of "model *F* value" because the probability of this occurring is only 0.01%. The *P* value obtained is extremely small (Prob. >*F*) which shows that the corresponding coefficient is significant and so its played a part in the response variable. The *P*-value for the density model is less than 0.05, hence, it is considered significant. For a *P*-value to be insignificant, it must be greater than 0.100. However, it was observed that four factors term (A, B, AB and A^2) are the most significant model terms from the ANOVA analysis (density measurement). This is because their *P*-values is less than 0.05 and their influence on density is at >95% confidence level. The *P*-value of B^2 is greater than 0.05 (0.3138) which indicate that its influence on the response model is statistically insignificant. The reduction of response variability was measured to be 0.9984 using R^2 (coefficient of determination). This is an indication that experimental variables contributed 99.84% to the total variance in the density measurement. The R^2 is very close to 1, which is an indication that best fit of data is used for the model. The standard deviation (SD) for density measurement model is 0.1188.

Kumar et al. [36] reported that lower SD value and the closeness of R^2 value to unity resulted to a better model. This mean that the predicted value is very close to the actual value (response). In this study, the difference between the adjusted value (0.9972) and the predicted value (0.9845) is < 0.2 (0.0127), thus, implying both are in agreement. The obtained adjusted coefficient of determination value for density measurement (Adj. R^2) is 0.9972. This is very high and signifies the important of the model for predictive

Table 4
ANOVA for the RSM quadratic model for density of IN738LC alloys using CCD.

Source	Sum of Squares	D_f	Mean Square	*F*-value	*P*-value	
Model	61.29	5	12.26	868.04	<0.0001	Significant
A-Temperature	57.66	1	57.66	4083.13	<0.0001	
B-Pressure	1.40	1	1.40	99.26	<0.0001	
AB	0.3600	1	0.3600	25.49	0.0015	
A^2	1.46	1	1.46	103.54	<0.0001	
B^2	0.0166	1	0.0166	1.18	0.3138	
Residual	0.0989	7	0.0141			
Lack of fit	0.0989	3	0.0330			
Pure error	0.0000	4	0.0000			
Cor total	61.39	12				

R^2; 0.9984, adjusted R^2; 0.9972, adequate precision; 88.7713.

Table 5
Fit statistical parameters of the model equation obtained from ANOVA models for density of IN738LC alloys.

Type of variable	
Standard deviation (SD)	0.1188
Mean	95.61
Coefficient of variation C.V (%)	0.1243
Prediction error sum of square (PRESS)	0.9542
R^2	0.9984
Adjusted R^2	0.9972
Predicted R^2	0.9845
Adequate Precision	88.7713

purpose. The adequate precision value is 88.7713, which demonstrate that the model is fit for the process. The term "Adequate precision" is very important as it measure the signal to noise ratio. Thus, a value > 4 is required for a good model and this agreed with the value obtained in this study (88.7713). The value for this term was computed by dividing the difference between the maximum and minimum predicted response by the average SD of all the predicted response. Therefore, the obtained result indicates that the model is good for the design. The C.V observed is 0.1243% which is very low and signifies that the experimental results is satisfactory. There is no data recorded for the *P*-value of the lack of fit test, indicating that its fall within the insignificant range relative to pure error. This means that the model is accurate with the experimental data. Therefore, the quadratic model used for predicting the density property of SPS-ed IN738LC superalloy as a function of temperature (A) and pressure (B) is given in terms of coded factors as given by Equation (3).

$$\text{Density} = -42.53333 + 0.203069A + 0.440402B - 0.00300AB - 0.000073A^2 - 0.000776B^2 \quad (3)$$

3.4. The normal probability plot of residuals and plots of density measurement

The normal plot of the residuals (density) and the relationship between the actual response versus predicted response plots (density) for interpreting the adequacy of the developed model are presented in Fig. 4a and b. The difference between the actual responses and the predicted responses is known as residuals. Hence, the deviation between the actual values and the predicted values are represented in the normal probability plot of residual. For a model to be adequate, the points on the normal probability plot of the residuals should form a straight line. When such pattern is observed on a normal plot of residuals, it can be said that the residual forms a normal distribution and the errors are randomly distributed. Likewise, the residual points are well aligned. A weak model will display an irregular pattern or non-linear pattern in the residuals versus predicted response plots. It was observed that the input parameters formed a model, such that the predicted responses are in conformity with the actual values. In addition, the plots show that the values of R^2 (0.9984), R^2 adj (0.9972) and the residual analysis appropriately fit the model to the experimental data. Therefore, Fig. 4a and b can be interpreted as the stochastic error and deterministic portion for IN738LC alloys density for normal residual plots coupled with the actual values versus the predicted values respectively. The contour and the 3D plot showing the interactive effects of the pressure and the temperature on the density of IN738LC alloy is presented in Figs. 5 and 6 respectively. The density increased with increasing sintering temperature and pressure. At the least value of temperature and pressure, small value of density (92%) was obtained and indicated by the blue colour on the graph. The highest density was obtained at the highest temperature (98%). The increased sintering temperature enhanced diffusion and consolidation of powders, whereby, pores are rapidly closed, leading to porosity reduction and microstructure refinement. Tushar and Rajarshi [37], investigated the effect of processing parameters (temperature and pressure) on microstructure and mechanical properties of nickel, using SPS method. They observed than increase in sintering temperature from 700 to 1000 °C and pressure range of 130–278 MPa resulted to increased density, ductility and strength of the sintered metal. These was also corroborated by other researchers [38,39]. Table 6 shows the values of the predicted density (numerical), actual density (experimental) and the percentage error between the two parameters. The comparison between the experimental relative density and the RSM predicted density is presented in Fig. 7. Marginal deviation was observed between the experimental relative density values and the predicted relative density values. Thus, the developed model is suitable to adequately predict the SPS-ed IN738LC material property (density).

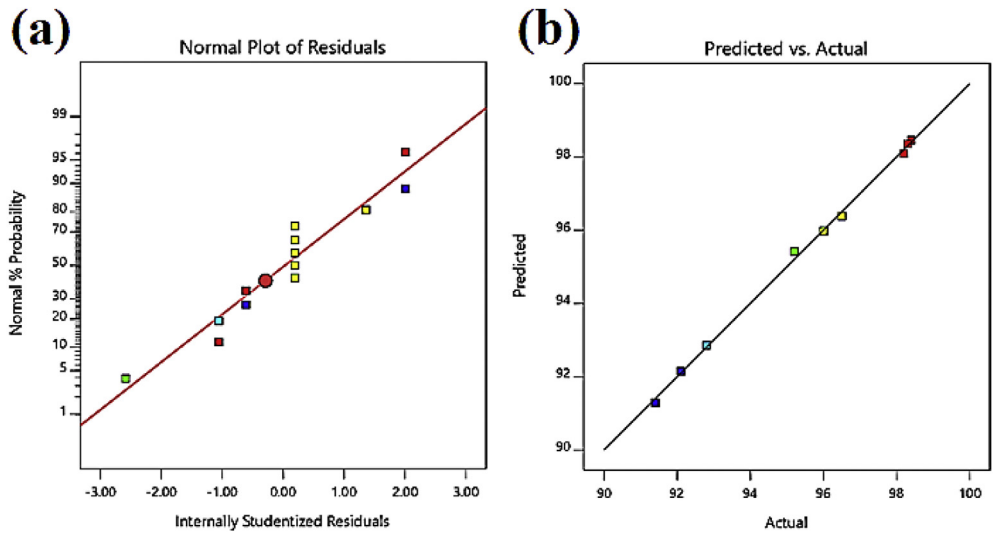

Fig. 4. Deterministic portion and stochastic error for the density property of IN738LC alloys. (a) The normal plot of residuals. (b) The predicted versus actual values (response).

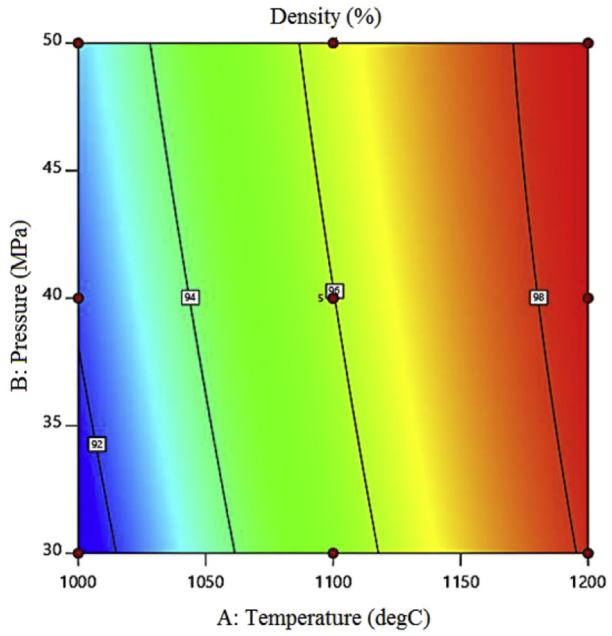

Fig. 5. The contour plot of density with respect to temperature and pressure of IN738LC alloy.

3.5. ANOVA analysis and model fitting for hardness of IN738LC alloy

The ANOVA analysis of the model for hardness property as obtained from RSM is presented in Tables 7 and 8. It was observed that the *F* value is 14972.27 and this indicates that the model is significant. The implication of this observation has been explained from the density results because both outcomes followed similar trend. The possibility of having a large number (14972.27) for "model *F* value" due to noise is only 0.0001. The contribution of *P* value to the response variable values is less than 0.500 (*P* value, < 0.0001) which suggest that the model and the model terms are significant. This also occurred for temperature (A) and pressure (B) which made them significant to the hardness property of 1N738LC alloys. For a value greater than 0.10, it is termed insignificant. Therefore, both A and B formed part of the equation that govern the model. The lack of fit is not significant, because there is no value obtain for it and this is necessary for the developed model to fit appropriately. The coefficient of determination (R^2) is closer to 1 (0.9997), indicating that 99.97% of the total variance in the hardness measurement contributed to the experimental variables. It can be said that the value obtained for the model is sufficient without any need for additional terms because the value of (R^2) adj. Is almost 1 (0.9996). The smaller value of the standard deviation (0.3847) also attest to the quality of the model, suggesting that there is limited error and high accuracy between the predicted values and the actual values. The difference between the adjusted value (0.9996) and the predicted value (0.9997) is minimal which shows that both are reasonably in agreement. The signal to noise ratio measured by the adequate precision parameter is greater than 4 (300.3464) and this signifies that there is adequate signal and the model can be used to navigate space. Hence, the quadratic model used for predicting the hardness property of the SPS-ed IN738LC superalloy as a function of temperature (A) and pressure (B) is given in terms of coded factors in Equation (4).

Table 6
Experimental relative density (actual) and RSM statistical relative density (predicted) of IN738LC alloy.

Runs	Factors		Actual Density (%)	Predicted Density (%)	Error (%)
	Temperature A (°C)	Pressure B (MPa)			
1	1000	30	91.40	91.29	−0.11
2	1000	40	92.10	92.15	0.05
3	1000	50	92.80	92.86	0.06
4	1100	30	96.00	95.98	−0.02
5	1100	40	96.50	96.39	−0.11
6	1100	40	96.00	95.98	−0.02
7	1100	40	96.00	95.98	−0.02
8	1100	40	96.00	95.98	−0.02
9	1100	40	95.20	95.42	0.22
10	1100	50	96.00	95.98	−0.02
11	1200	30	98.20	98.09	−0.11
12	1200	40	98.30	98.35	−0.05
13	1200	50	98.40	98.46	−0.06

$$\text{Hardness} = 33.03974 + 0.271733A + 0.058167B \quad (4)$$

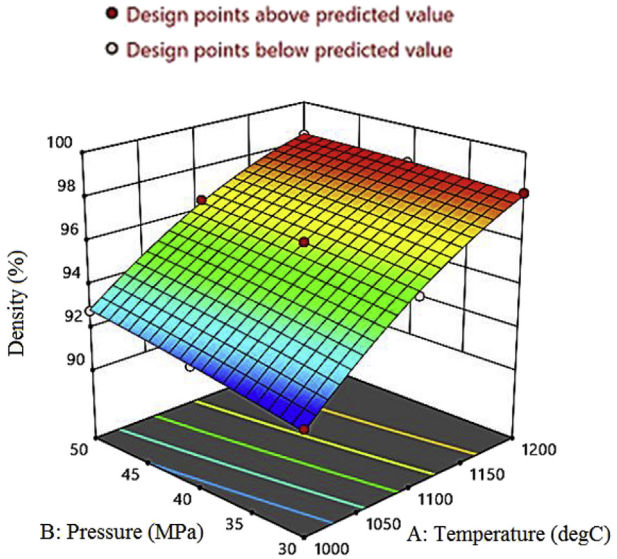

Fig. 6. 3D RSM plot of density with respect to temperature and pressure of IN738LC alloy.

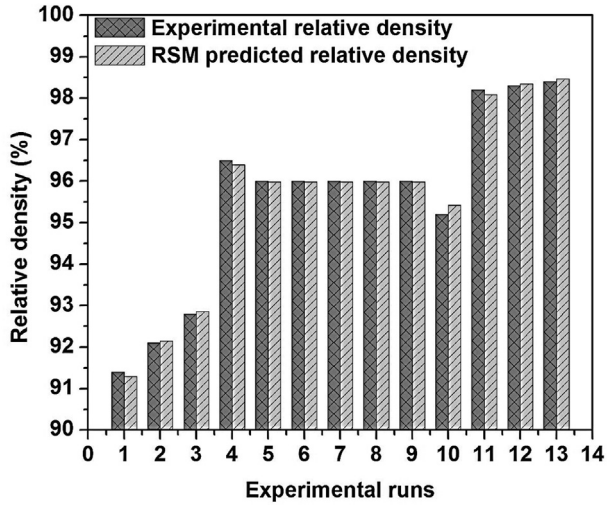

Fig. 7. Experimental relative density versus RSM predicted relative density of IN738LC alloy.

Table 7
ANOVA for the RSM quadratic model for hardness of IN738LC alloys using CCD.

Source	Sum of Squares	D_f	Mean Square	*F*-value	*P*-value	
Model	4432.37	2	2216.19	14972.27	<0.0001	significant
A-temperature	4430.34	1	4430.34	29930.82	<0.0001	
B-pressure	2.03	1	2.03	13.71	0.0041	
Residual	1.48	10	0.1480			
Lack of fit	1.48	6	0.2467			
Pure error	0.0000	4	0.0000			
Corr. Total	4433.85	12				

R^2; 0.9997, adjusted R^2; 0.9996, adequate precision; 300.3468.

Table 8
Fit statistical parameters of the model equation obtained from ANOVA models for hardness of IN738LC alloys.

Type of variable	
Standard Deviation (SD)	0.3847
Mean	334.27
Coefficient of variation CV (%)	0.1151
Prediction error sum of square (PRESS)	3.37
R^2	0.9997
Adjusted R^2	0.9996
Predicted R^2	0.9992
Adequate precision	300.3468

3.6. The normal probability plot of residuals and plots of hardness measurement

The normal plot of the residuals (hardness) and the relationship between the actual response versus predicted response plots (hardness) used for interpreting the adequacy of the developed model are presented in Fig. 8a and b. It is important that the values obtain in both predictive model and the experimental results are very close as this signifies the accuracy of the model. It was observed that the plots model ensured relatively even distribution of values along the fit line for the hardness responses. This was supported by the adj. R^2 (0.9996) and R^2 (0.9997) which ensure that the model is fit to the experimental data, due to their values getting close to 1. The contour and 3D plots for the response surface, showing the interaction between the two variables (temperature and pressure) and their effect on the hardness responses are presented in Figs. 9 and 10. It was clear that the sintering temperature has positive and major influence on the hardness responses while pressure has marginal effect. The higher the temperature, the higher the hardness property. The sintering temperature of 1200 °C resulted to maximum hardness property, corresponding to 362.03 HV (Fig. 9, Table 9). Small value of sintering temperature resulted to smaller value of the hardness property corresponding to 306.52 HV (Fig. 9, Table 9). Thus, the optimization focus in terms of temperature and pressure should be in the region where higher property is obtained. The observation of hardness property in this study is similar to reported result in literature [38,40]. When the density of sintered alloy increases with increasing temperature and pressure, the hardness follows the same trend. The experimental and the RSM predicted values of hardness property is presented in Table 9. The plot of the predicted numerical values from the developed model and the experimental values of hardness property is presented in Fig. 11. It was observed that the experimental values agreed significantly with the predicted values showing minimal error between them (Table 9). This confirmed that the model is good for predicting the hardness values of IN738LC alloy.

3.7. Confirmation studies of the density and hardness properties of IN738LC alloy

The adequacy of the statistical models and the 3D response surface generated during the optimization processes using design of expert software was verified. This is to understand the optimal combination of variables that led to satisfactory responses [41]. Fifteen (15) optimal responses were obtained. The selection constraints in this study was based on the SPS principle which require that the alloy is sintered at a temperature below its the melting temperature [12]. The fifteen runs were presented in Table 10. Ideally, the desirability value ranges of response should be from 0 to

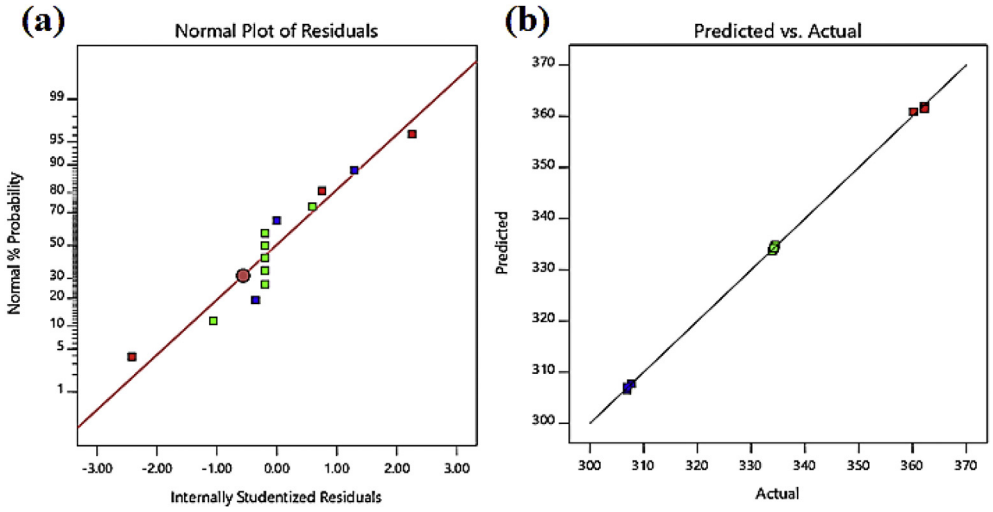

Fig. 8. Deterministic portion and stochastic error for the hardness property of IN738LC alloys. (a) The normal plot of residuals. (b) The predicted versus actual values (response).

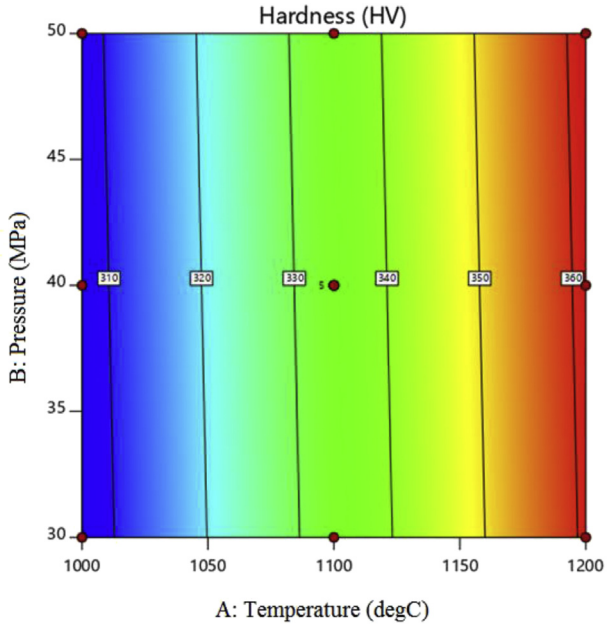

Fig. 9. The contour plot of hardness values with respect to temperature and pressure of IN738LC alloy.

1. From Table 10, the optimal combinations of temperature and pressure that yielded better properties (density and hardness) of IN738LC alloy and gave a desirability values that is approximated to 1 was selected. The results obtained (15 runs) signifies that the confirmation study is ideal. The selected solution out of the fifteen runs to determine the best desirability range is presented in Fig. 12. Therefore, the desirability value that is closest to 1 is selected based on the DOE software. These is the combination of variables comprising of 1200 °C temperature and 50 MPa pressure with corresponding density of 98.457% and hardness of 362.028Hv.

3.8. Microstructural analysis

Density is a vital material property that influences the mechanical properties of metallic alloys [42]. According to the DOE

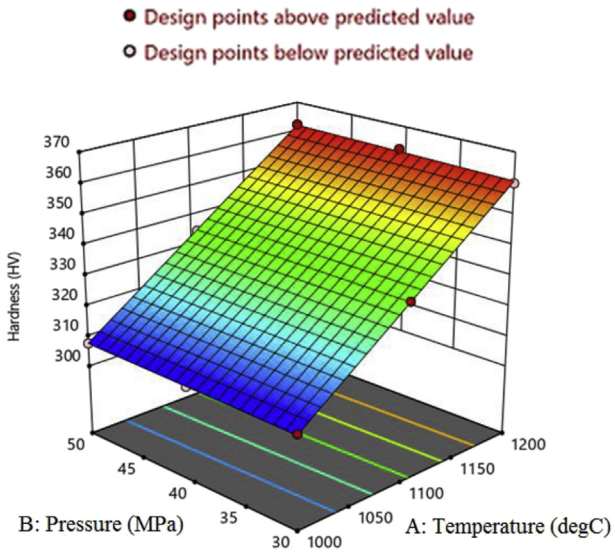

Fig. 10. 3D RSM plot of hardness with respect to temperature and pressure of IN738LC alloy.

Table 9
Experimental relative hardness (actual) and RSM statistical relative hardness (predicted).

Runs	Factors		Actual Hardness (HV)	Predicted Hardness (HV)	Error
	Temperature A (°C)	Pressure B (MPa)			
1	1000	30	306.90	306.52	−0.38
2	1000	40	306.98	307.10	0.12
3	1000	50	307.68	307.68	0.00
4	1100	30	334.20	334.27	0.07
5	1100	40	334.50	334.85	0.35
6	1100	40	334.20	334.27	0.07
7	1100	40	334.20	334.27	0.07
8	1100	40	334.20	334.27	0.07
9	1100	40	333.89	333.69	−0.2
10	1100	50	334.20	334.27	0.07
11	1200	30	360.15	360.86	0.71
12	1200	40	362.20	361.45	−0.75
13	1200	50	362.25	362.03	−0.22

(RSM) and experimental study of IN738LC alloys, increased percentage relative density was obtained with increasing sintering temperature and pressure. Since minimal changes was observed with the applied pressure, and from the desirability result of the DOE runs, the focus is on the influence of sintering temperature because its shows greater effect on the density and hardness properties. In order to understand the effect of sintering temperatures (1000, 1100 and 1200 °C) on the microstructure of the optimized IN738LC alloy at a fixed pressure of 50 MPa, the SEM analysis was conducted. This is presented in Figure 13 (a, b, c), respectively. The three images represent an unetched microstructure of IN738LC alloys. Pores formation were visible within the microstructure of the three alloys. The pores were of different shapes, sizes and were heterogeneously distributed within the microstructure. They were close to each other, especially for the alloy sintered at 1000 °C.

The quantification of the porosity, both from the DOE (RSM) and the experimental study shows that increase in sintering temperature resulted to increased relative density. The increasing relative density signifies that the percentage porosity reduces with increasing sintering temperature. In the SPS technology, it has been established that high sintering temperature causes local temperature gradients (temperature between particles contact) which aided grain boundary softening and consolidation enhancement

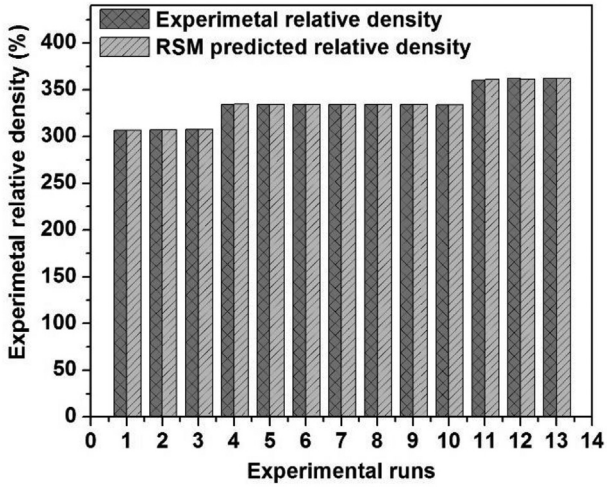

Fig. 11. Experimental hardness versus RSM predicted hardness of IN738LC alloy.

Table 10
Optimum combinations of optimization on density and hardness properties of IN738LC alloy.

Runs	Temperature (°C)	Pressure MPa	Density (%)	Hardness (HV)	Desirability	
1	1200.000	50.000	98.457	362.028	0.998	Selected
2	1200.000	49.174	98.455	361.980	0.998	
3	1200.000	48.339	98.451	361.931	0.997	
4	1200.000	48.233	98.450	361.925	0.997	
5	1200.000	48.076	98.449	361.916	0.997	
6	1200.000	47.920	98.448	361.907	0.997	
7	1200.000	47.611	98.446	361.889	0.997	
8	1200.000	47.492	98.446	361.882	0.997	
9	1200.000	46.845	98.441	361.844	0.996	
10	1200.000	46.122	98.435	361.802	0.996	
11	1200.000	46.044	98.434	361.798	0.996	
12	1200.000	45.671	98.431	361.776	0.996	
13	1200.000	43.199	98.402	361.632	0.994	
14	1200.000	37.905	98.310	361.325	0.985	
15	1200.000	33.638	98.204	361.076	0.975	

through thermal diffusion [43]. This led to shrinkage of the bulk material by ensuring that the pores within the grain and along the grain boundaries are closed, which in turn reduces the level of porosity in a material. Therefore, porosity decreases with increasing sintering temperature at a fixed pressure because diffusion (grain boundary or lattice diffusion) is known to be temperature dependent phenomena [38]. The higher value of the density obtained for sample sintered at 1200 °C is a function of the sintering temperature used in this study. This increases the heat energy during sintering and the diffusion path which resulted to increase in density. This ensure that pores that are trapped within the grain are rapidly closed and porosity reduce [44]. Visual observation of the three micrographs shows that sample processed at 1200 °C have lower porosity as expected and the pores are relatively far apart (Fig. 13c). Relatively large areas that are pore free can be observed for the sample sintered at 1200 °C. This agrees with the porosity and percentage relative density values evaluated and therefore, denser microstructure enhances hardness property.

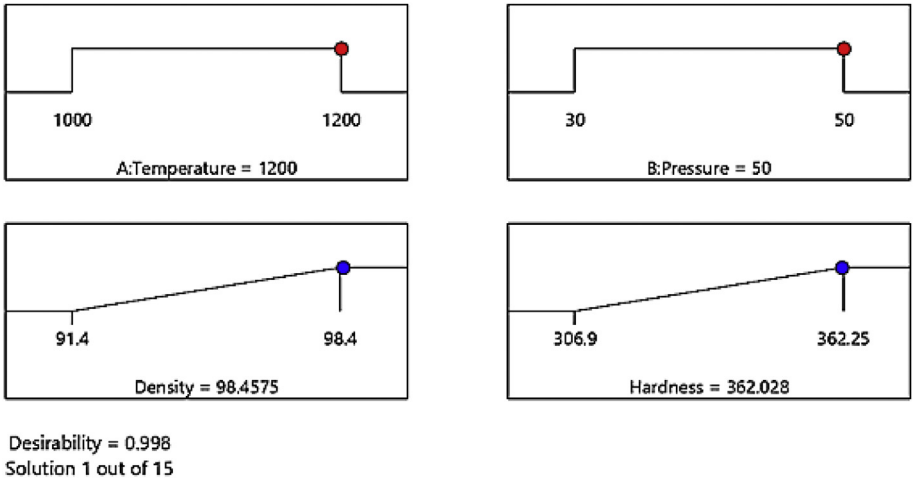

Fig. 12. Selected solution for the desirability study.

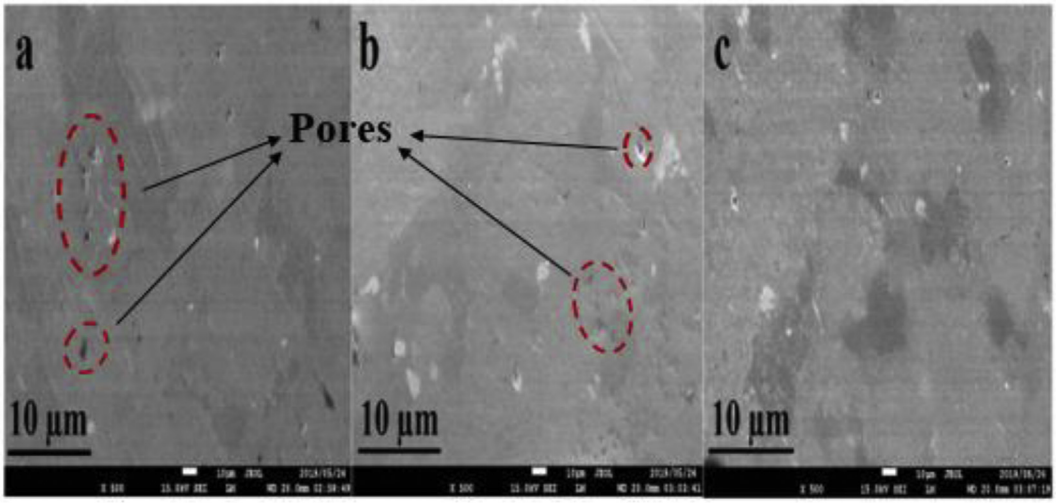

Fig. 13. Unetched micrographs (SEM) for IN738LC alloys. (a) Alloy processed at 1000 °C temperature and 50 MPa pressure, (b) alloy processed at 1100 °C temperature and 50 MPa pressure, (c) alloy processed at 1200 °C temperature and 50 MPa pressure.

4. Conclusion

The influence of processing parameters of SPS (temperature and pressure) on the material and mechanical properties (density and hardness) of IN738LC alloy was investigated. Alloy with good properties was successfully obtained through the implementation of systematic procedures of Response Surface Methodology (RSM) standard from the design of experiment approach. Within the range of this study, the statistical analysis results show that sintering temperature is the controlling variable that influences the obtained properties of IN738LC alloys. The investigative interaction of both sintering temperature and pressure indicates that the increased density and hardness properties is as a result of increasing temperature and pressure. The temperature of 1200 °C and pressure of 50 MPa with corresponding percentage relative density of 98.457% and hardness of 362.028 HV were the optimal values obtained, based on the RSM optimization design. There was marginal difference between the experimental results and the optimized results which suggest that the model is reliable. Therefore, the obtained results show a negligible error between the experimental and the optimized results. The percentage porosity obtained (percentage theoretical density minus both optimized and experimental density) show that good densification and hardness properties was achieved. The model through the Design Expert software developed two empirical formulas for both density and hardness properties with respect to the sintering temperature and pressure and their corresponding coefficients of independent variables. Thus, optimization helps to reduce numbers of trials and present at a glance the interactive combination of process parameters and their effects on responses (output). ANOVA analysis presented show that the developed model from RSM and CCD was statistically adequate.

Conflicts of interest

The authors declare that there is no conflicts of interest.

Acknowledgements

This work is funded by the Research and Innovation Directorate of Tshwane University of Technology and supported in part, by the Department of Mechanical Engineering, Mechatronics and Industrial Design, Institute for NanoEngineering Research (INER), Department of Chemical, Metallurgical and Materials Engineering and the Faculty of Engineering and Built Environment of the Tshwane University of Technology, Pretoria, South Africa.

References

[1] D. Rajamani, et al., Experimental investigation and optimization of PAC parameters on Monel 400™ superalloy, Mater. Manuf. Process. 33 (16) (2018) 1864–1873.
[2] Y. Sato, et al., Microstructure and mechanical properties of friction stir welded SAF 2507 super duplex stainless steel, Mater. Sci. Eng. A 397 (1–2) (2005) 376–384.
[3] B. Rossi, Discussion on the use of stainless steel in constructions in view of sustainability, Thin Walled Struct. 83 (2014) 182–189.
[4] Y. Chen, C. Bunget, L. Mears, et al., Investigations in subsurface damage when machining γ′-strengthened nickel-based superalloy, Proc. Inst. Mech. Eng., Part B: J. Eng. Manuf. 230 (7) (2016) 1221–1233.
[5] E. Akca, A. Gürsel, A review on superalloys and IN718 nickel-based INCONEL superalloy, Period. Eng. Nat. Sci. 3 (1) (2015).
[6] V. Maleki, H. Omidvar, M.-r. Rahimipour, Effect of gap size on microstructure of transient liquid phase bonded IN-738LC superalloy, Trans. Nonferrous Metals Soc. China 26 (2) (2016) 437–447.
[7] A. Golezani, M. Bageri, R. Samadi, Microstructural change and impact toughness property of Inconel 738LC after 12 years of service, Eng. Fail. Anal. 59 (2016) 624–629.
[8] S. Rani, A.K. Agrawal, V. Rastogi, Failure analysis of a first stage IN738 gas turbine blade tip cracking in a thermal power plant, Case Stud. Eng. Fail. Anal. 8 (2017) 1–10.
[9] Z. Fu, et al., Microstructure and strengthening mechanisms in an FCC structured single-phase nanocrystalline Co25Ni25Fe25Al7.5Cu17.5 high-entropy alloy, Acta Mater. 107 (2016) 59–71.
[10] N. Saheb, et al., Spark plasma sintering of metals and metal matrix nanocomposites: a review, J. Nanomater. 2012 (2012) 18.
[11] N. Ghosh, S. Harimkar, Consolidation and synthesis of MAX phases by spark plasma sintering (SPS): a review, in: Advances in Science and Technology of Mn+ 1axn Phases, Elsevier, 2012, pp. 47–80.
[12] Z. Munir, U. Anselmi-Tamburini, M. Ohyanagi, The effect of electric field and pressure on the synthesis and consolidation of materials: a review of the spark plasma sintering method, J. Mater. Sci. 41 (3) (2006) 763–777.
[13] C. Manière, et al., Spark plasma sintering and complex shapes: the deformed interfaces approach, Powder Technol. 320 (2017) 340–345.
[14] C. Manière, E. Torresani, E.A. Olevsky, Simultaneous spark plasma sintering of multiple complex shapes, Materials 12 (4) (2019) 557.
[15] M. Suárez, et al., Challenges and Opportunities for Spark Plasma Sintering: a Key Technology for a New Generation of Materials, InTech, 2013.
[16] C. Ujah, O. Popoola, V. Aigbodion, Optimisation of spark plasma sintering parameters of Al-CNTs-Nb nano-composite using Taguchi Design of Experiment, Int. J. Adv. Manuf. Technol. 100 (5–8) (2019) 1563–1573.
[17] A. Mohammadzadeh, et al., On the physical and mechanical properties of spark plasma sintered pure Ti and Ti-TiB composite, Mater. Res. Express 5 (12) (2018) 126512.
[18] M.A. Sayed, et al., Application of Taguchi method in optimization of process parameters of ODS tungsten heavy alloys, Adv. Mater. Res. 6 (1) (2017) 79–91.
[19] M. Khajelakzay, S.R. Bakhshi, Optimization of spark plasma sintering parameters of Si3N4-SiC composite using response surface methodology (RSM), Ceram. Int. 43 (9) (2017) 6815–6821.
[20] Z. Ahmadi, et al., Densification improvement of spark plasma sintered TiB2-based composites with micron-, submicron-and nano-sized SiC particulates, Ceram. Int. 44 (10) (2018) 11431–11437.
[21] M.S. Asl, et al., Contribution of SiC particle size and spark plasma sintering conditions on grain growth and hardness of TiB2 composites, Ceram. Int. 43 (16) (2017) 13924–13931.
[22] Z. Balak, M. Zakeri, Application of Taguchi L32 orthogonal design to optimize flexural strength of ZrB2-based composites prepared by spark plasma sintering, Int. J. Refract. Metals Hard Mater. 55 (2016) 58–67.
[23] Z. Balak, et al., Optimization of effective parameters on thermal shock resistance of ZrB2-SiC-based composites prepared by SPS: using Taguchi design, Mater. Chem. Phys. 196 (2017) 333–340.
[24] Z. Li, et al., Optimising the process parameters of selective laser melting for the fabrication of Ti6Al4V alloy, Rapid Prototyp. J. 24 (1) (2018) 150–159.
[25] V. Aggarwal, S.S. Khangura, R. Garg, Parametric modeling and optimization for wire electrical discharge machining of Inconel 718 using response surface methodology, Int. J. Adv. Manuf. Technol. 79 (1–4) (2015) 31–47.
[26] A. Tiwary, B. Pradhan, B. Bhattacharyya, Study on the influence of micro-EDM process parameters during machining of Ti–6Al–4V superalloy, Int. J. Adv. Manuf. Technol. 76 (1–4) (2015) 151–160.
[27] Y. Zhou, et al., Modelling and optimisation of surface roughness from microgrinding of nickel-based single crystal superalloy using the response surface methodology and genetic algorithm, Int. J. Adv. Manuf. Technol. 85 (9–12) (2016) 2607–2622.
[28] Z. Zhang, et al., Mechanical behavior of cryomilled Ni superalloy by spark plasma sintering, Metall. Mater. Trans. A 40 (9) (2009) 2023–2029.
[29] M. Naebe, K. Shirvanimoghaddam, Functionally graded materials: a review of fabrication and properties, Appl. Mater. Today 5 (2016) 223–245.
[30] S. Ma, et al., Effects of temperature on microstructure and mechanical properties of IN718 reinforced by reduced graphene oxide through spark plasma sintering, J. Alloy. Comp. 767 (2018) 675–681.
[31] M. Kolahdoozan, F. Azimifar, R. Yazdi, Finite element investigation and optimization of tool wear in drilling process of difficult-to-cut nickel-based superalloy using response surface methodology, Int. J. Adv. Des. Manuf. Technol. 7 (2) (2014).
[32] B. Davoodi, A. Hosseini Tazehkandi, Cutting forces and surface roughness in wet machining of Inconel alloy 738 with coated carbide tool, Proc. Inst. Mech. Eng. B J. Eng. Manuf. 230 (2) (2016) 215–226.
[33] M.I. Makena, et al., Effect of sintering parameters on densification, corrosion and wear behaviour of Ni-50Fe alloy prepared by spark plasma sintering, J. Alloy. Comp. 699 (2017) 1166–1179.
[34] S. Yan, et al., Fabrication of highly compact Inconel 718 alloy by spark plasma sintering and solution treatment followed by aging, Vacuum 163 (2019) 194–203.
[35] O. Guillon, et al., Field-assisted sintering technology/spark plasma sintering: mechanisms, materials, and technology developments, Adv. Eng. Mater. 16 (7) (2014) 830–849.
[36] A. Kumar, H. Singh, V. Kumar, Study the parametric effect of abrasive water jet machining on surface roughness of Inconel 718 using RSM-BBD techniques, Mater. Manuf. Process. 33 (13) (2018) 1483–1490.
[37] T. Borkar, R. Banerjee, Influence of spark plasma sintering (SPS) processing parameters on microstructure and mechanical properties of nickel, Mater. Sci. Eng. A 618 (2014) 176–181.
[38] M.B. Shongwe, et al., Effect of sintering temperature on the microstructure and mechanical properties of Fe–30% Ni alloys produced by spark plasma sintering, J. Alloy. Comp. 649 (2015) 824–832.

[39] M.S. Asl, et al., Effects of sintering temperature on microstructure and mechanical properties of spark plasma sintered titanium, Mater. Chem. Phys. 203 (2018) 266–273.
[40] Y. Zhang, et al., High strength bulk tantalum with novel gradient structure within a particle fabricated by spark plasma sintering, Mater. Sci. Eng. A 528 (29–30) (2011) 8332–8336.
[41] S. Ramesh, L. Karunamoorthy, K. Palanikumar, Measurement and analysis of surface roughness in turning of aerospace titanium alloy (gr5), Measurement 45 (5) (2012) 1266–1276.
[42] S. Diouf, A. Molinari, Densification mechanisms in spark plasma sintering: effect of particle size and pressure, Powder Technol. 221 (2012) 220–227.
[43] E.A. Olevsky, L. Froyen, Impact of thermal diffusion on densification during SPS, J. Am. Ceram. Soc. 92 (2009) S122–S132.
[44] R. Yamanoglu, et al., Characterisation of nickel alloy powders processed by spark plasma sintering, Powder Metall. 57 (5) (2014) 380–386.